J. Phys.: Condens. Matter **24** (2012) 195901 (10pp) doi:10.1088/0953-8984/24/19/195901

Collective phase-like mode and the role of lattice distortions at $T_N \sim T_C$ in RMn_2O_5 (R = Pr, Sm, Gd, Tb, Bi)

Néstor E Massa[1], Ali F García-Flores[2], Domingos De Sousa Meneses[3], Leire del Campo[3], Patrick Echegut[3], Gilberto F L Fabbris[4], María Jesús Martínez-Lope[5] and José Antonio Alonso[5]

[1] Laboratorio Nacional de Investigación y Servicios en Espectroscopía Óptica-Centro CEQUINOR, Universidad Nacional de La Plata, CC 962, 1900 La Plata, Argentina
[2] Instituto de Física 'Gleb Wataghin', Universidade Estadual de Campinas, 13083-970 Campinas, São Paulo, Brazil
[3] CNRS-Conditions Extrêmes et Matériaux Haute Température et Irradiation, 1D, Avenue de la Recherche Scientifique, F-45071 Orléans, France
[4] Department of Physics, Washington University in St Louis, St Louis, MO 63130-4899, USA
[5] Instituto de Ciencia de Materiales de Madrid, CSIC, Cantoblanco, E-28049 Madrid, Spain

E-mail: neemmassa@gmail.com

Received 4 November 2011, in final form 23 February 2012
Published 17 April 2012
Online at stacks.iop.org/JPhysCM/24/195901

Abstract
We report on electronic collective excitations in RMn_2O_5 (R = Pr, Sm, Gd, Tb) showing condensation starting at and below $\sim T_N \sim T_C \sim 40$–$50$ K. Their origin is understood as partial delocalized e_g electron orbitals in the Jahn–Teller distortion of the pyramid dimer with strong hybridized Mn^{3+}–O bonds. Our local probes, Raman, infrared, and x-ray absorption, back the conclusion that there is no structural phase transition at $T_N \sim T_C$. Ferroelectricity is magnetically assisted by electron localization triggering lattice polarizability by unscreening. We have also found phonon hardening as the rare earth is sequentially replaced. This is understood as a consequence of lanthanide contraction. It is suggested that partially f-electron screened rare earth nuclei might be introducing a perturbation to e_g electrons prone to delocalize as the superexchange interaction takes place.

(Some figures may appear in colour only in the online journal)

1. Introduction

Strong fundamental interactions of complex oxides entangling charge, spins, lattice, and orbital distortions are part of a plethora of cooperative phenomena rich in novel properties. Compounds developing spontaneous electric polarization coexisting with magnetic order fall into this category. Supporting Jahn–Teller (JT) distortions and localized carriers, that might also order in stripes [1], they offer an attractive example for the study of basic interactions at an only energy scale. Congruent magnetic and lattice related phenomena provide grounds for a better understanding on the nature of elementary excitations emerging at magnetic–ferroelectric phase transitions, for which there is as yet no experimental consensus [2–6].

Ferroelectric materials have been described in the basic perovskite structure ABO_3. Below the Curie temperature T_C, they undergo a structural phase transition by which the lattice center inversion is lost and spontaneous electric polarization, i.e. ferroelectricity, sets in [7]. Although the phase transition may be broadly considered as displacive or order–disorder, more recent local structure studies suggest that real compounds share, to different degrees, properties belonging to both limits [8]. A characteristic hysteresis loop

develops in the ferroelectric state under an external electric field that mimics the magnetic susceptibility behavior in magnetically ordered systems [7].

Materials having simultaneous electric and magnetic order are called multiferroics. They have two order parameters, spontaneous polarization (antiferroelectric, ferroelectric, ferrielectric) and spontaneous magnetization (antiferromagnetism, ferromagnetism, ferrimagnetism), with one order triggering the other by magnetoelectric coupling. Multiferroics may be grouped depending on how close their lattice is to the perovskite structure. There are compounds with Bi or Pb at the A site. They have two valence electrons participating in chemical bonds through (sp)-hybridized states such as sp^2 or sp^3. These valence electrons in s-orbitals are the 'lone pair' electrons. The lone pair is unstable, mixing the $(ns)^2$ ground state and a low lying $(ns)^1(np)^1$ excited state, thus leading the ions to break the lattice inversion symmetry yielding ferroelectricity as in $BiFeO_3$ [9]. In this material the two 6s shell electrons of Bi^{3+} and the magnetic Fe^{3+} ions, at the A and B perovskite sites respectively, result in a compound within the framework of a 'proper' ferroelectric. On the other hand, those materials in which the electric polarization develops as consequence of multiple interactions that may include a pre-set magnetic order, are called 'improper' ferroelectrics. RMn_2O_5 (R = rare earth, Bi) belong to this last category [11].

From annoying impurity minor phases in the preparation of $RMnO_3$ (R = La, Pr, Nd), and isostructural to YMn_2O_5, the family of compounds RMn_2O_5 (R = rare earth, Bi) grew to be the source of much research activity due to their sharing of low temperature magnetic and ferroelectric ordering [12].

RMn_2O_5 (R = rare earth, Bi) are complex oxides containing manganese ions located in distinct crystallographic oxygen environments in a mixed valence state achieving stabilization of the nominal high spin oxidation states Mn^{3+} and Mn^{4+} [12, 13]. They have a lattice built on infinite chains of $Mn^{4+}O_6$ octahedra sharing edges linked by $Mn^{3+}O_5$ pyramid dimers. Bismuth and rare earth ions are in distorted RO_8 polyhedra, where Bi, unlike Pr, Sm, Gd, and Tb, has the two valence electrons in s-orbitals configuring the unstable lone electron pair [9, 14]. The octahedra–pyramid interconnection generates frustration in the spin structure since not all nearest neighbor Mn–O–Mn superexchange interactions are satisfied [15].

The motivation of the present work is the lack of agreement in understanding lattice order and the multiferroic nature of RMn_2O_5 (R = rare earth, Bi). While x-ray diffraction yields a centrosymmetric *Pbam*, $Z = 4$ space group from 300 to 4 K, the appearance of an effective antiferromagnetic order below $T_N \sim 39$–45 K, coexisting with spontaneous lattice polarization (ferroelectricity) a few degrees below T_C, implies an unobserved structural change with loss of the inversion center as in the $Pb2_1m$ subgroup of the space group *Pbam* [15–19]. The loss of the inversion center results in the positions for ions Mn2, O2, O3 and O4 split into two kinds of sites [20].

The same arguments apply for phonons measured independently in Raman and infrared spectra. These do not show the expected change due to the hypothetical gerade–ungerade split, meaning that infrared phonons also become Raman active and vice versa below $T_N \sim T_C$, predicted in the *Pbam* space group but absent in $P2_1am$ [21, 22]. At the transition temperatures, only very few uncorrelated and very weak new vibrational modes are detected at internal mode frequencies. Overall, the available data points for RMn_2O_5 (R = rare earth, Bi) suggest a lattice topology described by a unique space group above and below $T_N \sim T_C$.

We also report on temperature dependent collective electronic excitation in the 10–90 cm^{-1} frequency range in a temperature driven scenario triggering condensation at $T_N \sim T_C$. In addition, we found an unexpected oscillator mass dependence for vibrational modes, suggesting that rare earth nuclei may contribute as a perturbation source for the electronic cloud in a charge/orbital density wave scenario [23].

2. Experimental details

Our sample preparation follows procedures reported by Alonso *et al* [14]. Stoichiometric amounts of analytical grade R_2O_3 and $Mn(NO_3)_2 4H_2O$ were dissolved in citric acid. The citrate solutions were slowly evaporated and decomposed at temperatures up to 600 °C. All the organic materials were eliminated in a subsequent treatment at 800 °C in air. The samples were annealed at 1273 K either in a high oxygen pressure atmosphere (200 bar), for (R = Pr, Sm, Gd) or in air for (R = Tb, Bi) [12]. Our x-ray (Cu Kα) diffraction patterns for RMn_2O_5 (R = Bi, rare earth) are shown in figure 1.

Temperature dependent infrared reflectivity spectra with 2 cm^{-1} resolution were taken with polycrystalline pellets mounted on a cold finger of a home-made cryostat in a FT-IR Bruker 113v interferometer. A gold mirror was used as the 100% reference.

Raman scattering spectra were excited with the 514.5 nm laser line from an Ar^+ laser, with power of ~12 mW focused in a spot of ~100 μm diameter in a near back-scattering configuration. The scattered light was analyzed by a Jobin-Yvon triple grating spectrometer equipped with a LN_2-cooled CCD detector. The samples were mounted on the cold finger of a closed-cycle He refrigerator. All measurements were taken during heating runs.

We complemented those techniques with transmission-x-ray absorption measurements done at the D04B-XAFS2 beamline in the Brazilian Laboratory for Synchrotron Light (LNLS), adding local structural information on the long range averaging view of x-ray diffraction [12–14].

3. Results and discussion

3.1. Spin–phonon interactions

Early Raman scattering showed the presence of strong phonon modulation of the Mn–O–Mn magnetic superexchange electron correlations well above the magnetic ordering temperature at T_N [22, 24].

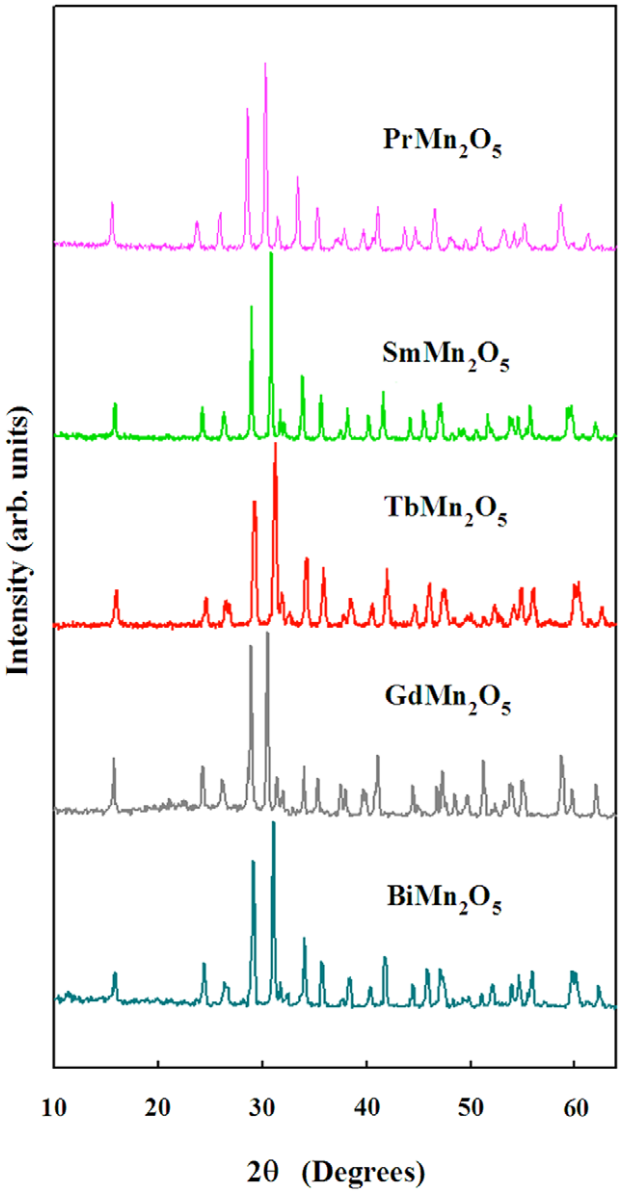

Figure 1. X-ray (Cu Kα) diffraction patterns for RMn_2O_5 (R = Bi, rare earth).

Raman band splits also hinted at a lower than expected lattice symmetry when the spectra of lighter lanthanide compounds were compared against those of heavier and Bi counterparts. Figures 2 and 3 show some new results in agreement with those findings.

The onset of the magnetoelastic effect on infrared active vibrational modes below $T^* \sim 65$ K is also shown in figure 4, where the temperature dependence of the internal stretching and bending phonon bands is found to have a turning point. At $\sim T_N$ the oscillator strength equation (6) (see below) diminishes as the samples cool down. This effect is better defined in $BiMn_2O_5$ [25], and shows that the displacement patterns modulating Mn–O–Mn [26] are common to infrared and Raman spectra. As pointed by García-Flores *et al* [22, 24], magnetic correlations couple to phonon frequencies through the superexchange integral associated with modulation of the Mn–O–Mn bonding angles and/or Mn–O stretching vibrations. It is also in agreement with results for $DyMn_2O_5$, reflecting the strong spin–lattice coupling dynamics above the magnetic ordering temperature [27].

3.2. Debye–Waller factors

Hints of lower lattice symmetry for rare earth heavier ions were corroborated by our study on the Bi first oxygen shell Debye–Waller factors.

Debye–Waller factors are shell dependent factors that are most sensitive to modes contributing to radial motions, basically depending only on the local vibrational structure. We studied nearest neighbor bismuth–oxygen pairs conforming to the asymmetric BiO_8 polyhedra to obtain information about the relative motion of atomic pairs in an analysis of extended x-ray absorption fine structure (EXAFS) spectra. The mean square variation in bond lengths is a quantity that has two components, one arising from the thermal vibrations and another from temperature dependent structural disorder [28].

We worked in the harmonic approximation, a single frequency Einstein approximation, not taking into account contributions from low structural disorder and dynamical effects due to ion motions. Then, the Debye–Waller factor applied to the Bi–O atomic pair reduces to

$$\sigma^2(T) = \sigma_0^2 + \left(\frac{\hbar^2}{2\mu k_B \theta_E}\right) \coth\left(\frac{\theta_E}{2T}\right) \qquad (1)$$

where σ_0^2 is the static contribution and θ_E is the so-called Einstein temperature for the ion pair with reduced mass μ. θ_E is the fitting parameter for the experimental data [28].

Its temperature dependence within that approximation shows no anomalies with distance distribution at about $T_N \sim 39$ K or elsewhere, showing that to achieve an acceptable fit to the experimental data it is only necessary to invoke one space group, in our case the orthorhombic *Pbam* [29]. Therefore, within our resolution ($\sim$0.01 Å), we could not identify any structural transition.

It does, however, establish the existence of two sets of Bi–O bonds. This is shown in figure 5 for the first bismuth coordination shell with two Einstein temperatures, $\theta_{E1} = 294 \pm 7$ K, for the four ions and $\theta_{E2} = 462 \pm 28$ K for the rest of the eight Bi–O bonds. Moreover, the relatively low values for θ_E also suggest that the polyhedra configuring the Bi–O first shell are not as rigid as Mn sublattices where θ_E ranges $\sim$700 K [29].

These results also corroborate earlier measurements by Tyson *et al* [30] for Tb in $TbMn_2O_5$, which found an anomalous Tb–O bond distribution that resolved into two peaks below $\sim$180 K, denoting inequivalent Tb sites away from the *Pbam* structure. This is an important departure from the results measured with diffraction patterns since it implies a lower symmetry space group than the fitted *Pbam*.

3.3. Far infrared reflectivity

Figures 6 and 7 show the near normal infrared reflectivity of RMn_2O_5 (R = Pr, Gd, Sm, Tb) from 300 to 4 K

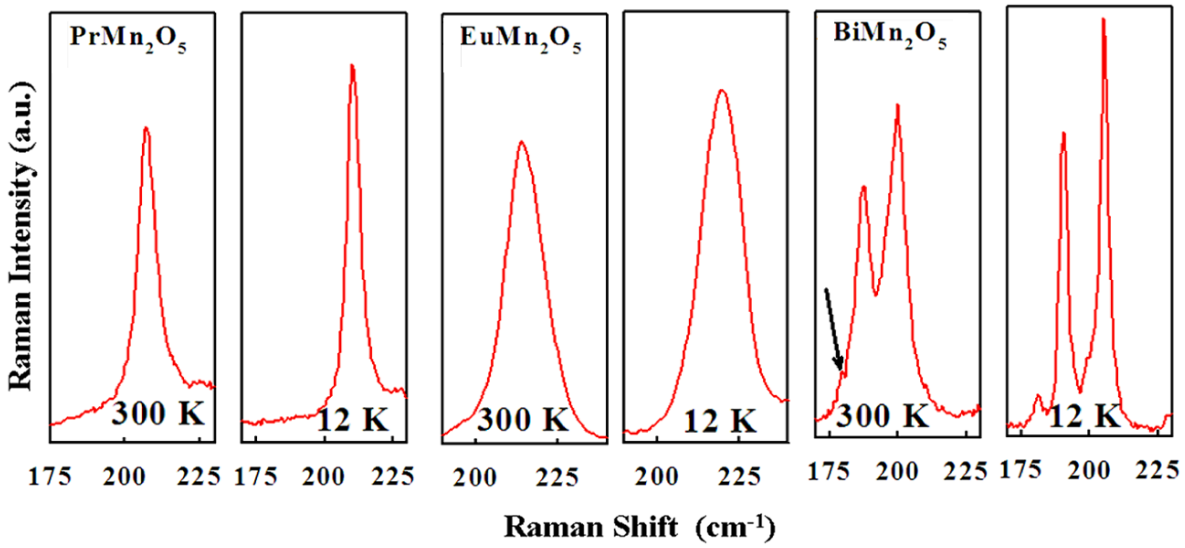

Figure 2. Raman spectra of the ∼200 cm^{-1} vibrational band in RMn_2O_5 (R = Pr, Eu, Bi) at 300 and 12 K. These suggest that replacements of lighter by heavier ions yields a lower space group symmetry even at 300 K. Note that in every case there is no change in the number of bands measured between 300 and 12 K.

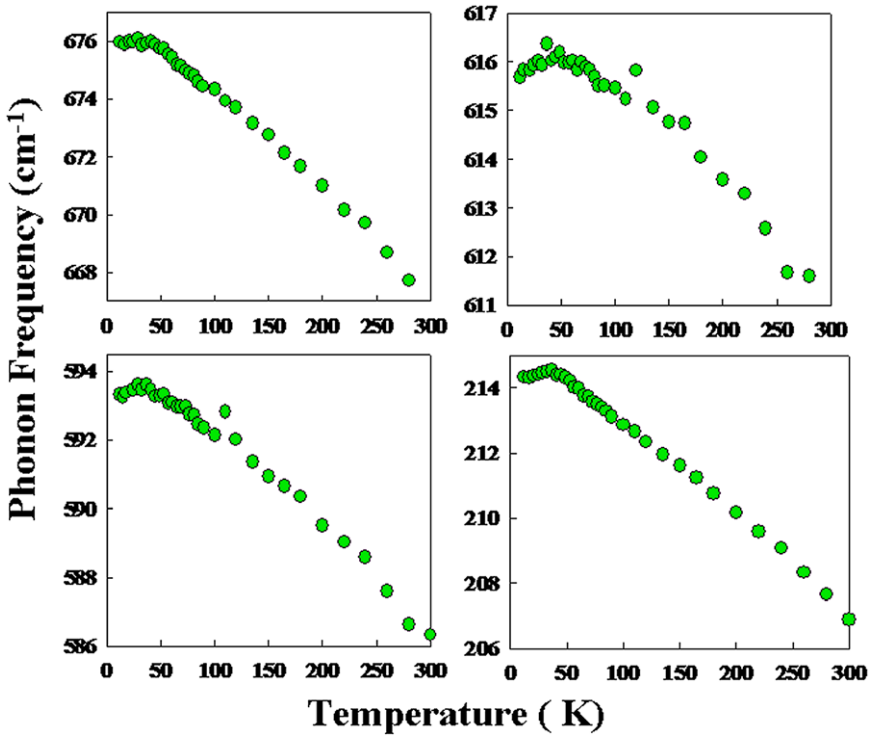

Figure 3. Temperature dependent Raman active $PrMn_2O_5$ phonons showing the effects of strong phonon modulation on the Mn–O–Mn magnetic superexchange electron correlations well above the magnetic ordering temperature at T_N.

in the 10–800 cm^{-1} frequency range. Lower frequency vibrational modes below ∼250 cm^{-1} correspond to the rare earth beating against polyhedra, while internal modes, antisymmetric stretching, bending and symmetric breathing modes are between ∼250 cm^{-1} and ∼600 cm^{-1} and ∼600 cm^{-1} and ∼770 cm^{-1}, respectively [27, 31]. The spectra show again that there are no substantial changes in the phonon profiles denoting a possible structural modification when phonon cooling and hardening take place.

In addition, a featureless band much stronger than any phonon structure appears below 100 cm^{-1}. Centered at ∼30 cm^{-1}, it is weakly temperature dependent down to $\sim T_N \sim T_C$, where it shows a smooth transition. We take it to originate from a collective electronic contribution. Its energy position and profile, and the absence of Raman activity in that frequency range, rule out possible contributions of rattling modes.

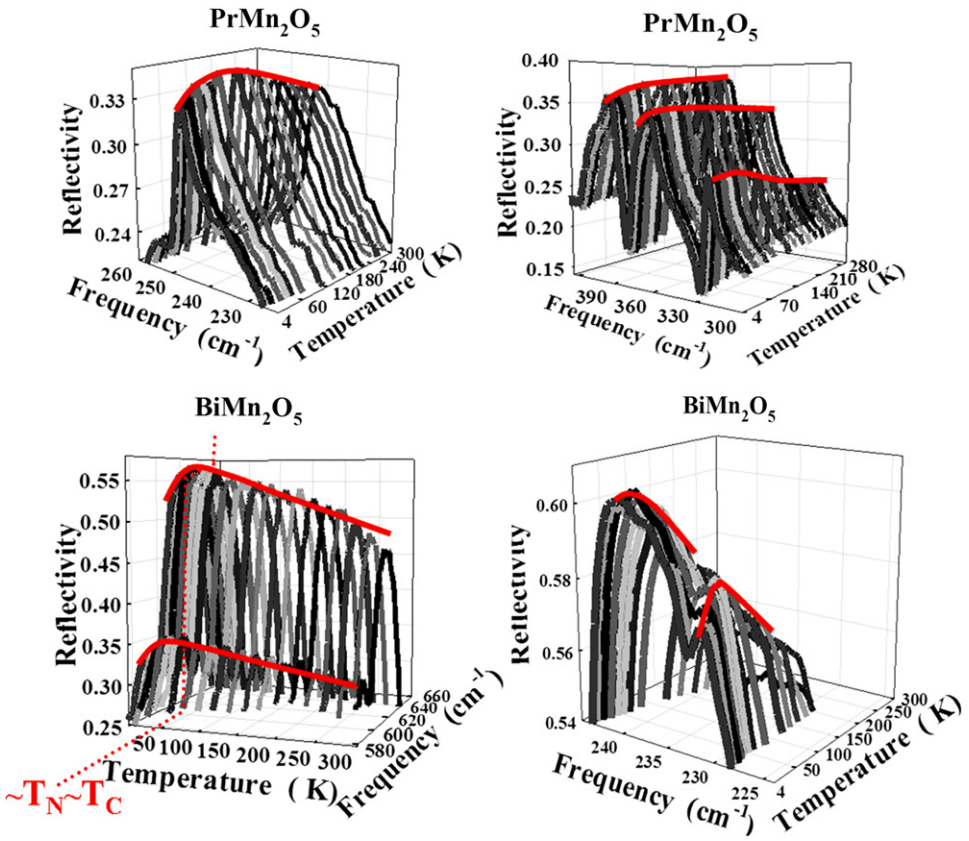

Figure 4. Vibrational bands for internal modes of $PrMn_2O_5$ and $BiMn_2O_5$ as a function of temperature showing the effect of magnetism in changes of the relative intensities (oscillator strengths) at and above the ordering temperatures. The continuous line on the top of the bands is a representation of the temperature dependence of the calculated oscillator strength (equation (6), see text).

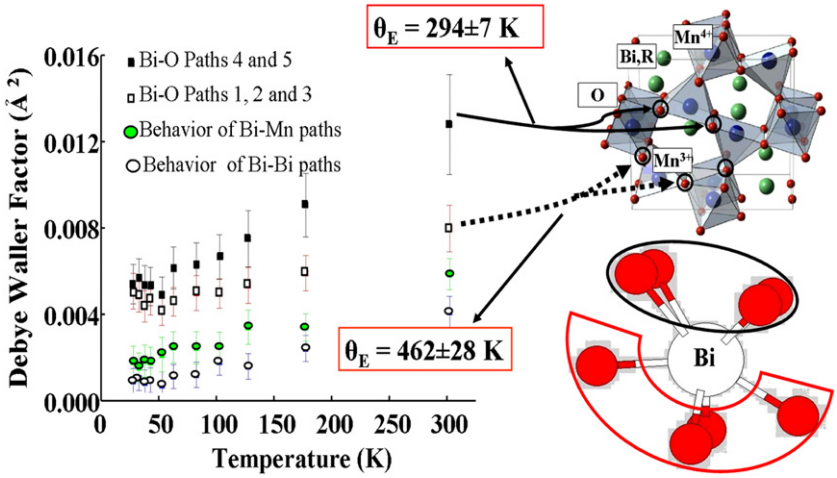

Figure 5. Temperature dependent Debye–Waller factors for $BiMn_2O_5$ showing two non-equivalent bond distances for Bi nearest neighbors in the BiO_8 sublattice cage. The right panel shows the two sets of Bi–O bonds in the $BiMn_2O_5$ lattice.

Figure 8 contrasts the overall spectra of $GdMn_2O_5$ against those of $BiMn_2O_5$ at 300 and 4 K. The smooth low frequency band against the discrete phonon spectrum is highlighted with circles. In $BiMn_2O_5$, the electronic configuration of Bi tends to further stabilize the lattice as the stereochemical activity of the Bi 6s lone pairs occurs on the orbitals [32]. This effect reduces that feature to a broad background on which, infrared spectroscopy being an additive technique, phonon profiles are delineated.

The temperature dependent detail of the low frequency reflectivities for $PrMn_2O_5$, $GdMn_2O_5$, $SmMn_2O_5$ and $TbMn_2O_5$ is shown in figure 9. We note that even if it seems to be rare earth dependent, the overall behavior is preserved showing lower temperature condensation, and thus electron localization. At about T_N, but at a slightly

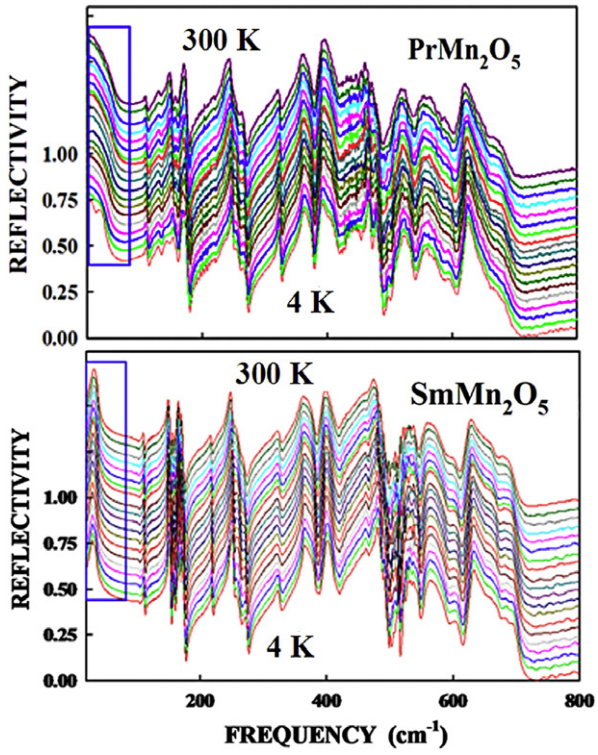

Figure 6. Temperature dependent near normal reflectivity of RMn_2O_5 (R = Pr, Sm) shown in increments of 10 K from 4 to 80 K and in increments of 20 K from 80 to 300 K. Rectangles highlight the low frequency phase-like mode. For better viewing the spectra have been displaced vertically.

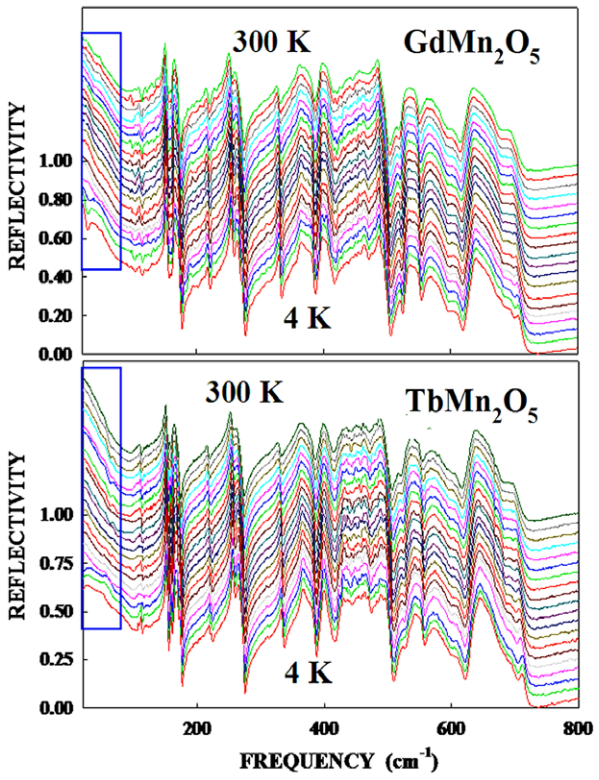

Figure 7. Temperature dependent near normal reflectivity of RMn_2O_5 (R = Gd, Tb) shown in increments of 10 K from 4 to 80 K and in increments of 20 K from 80 to 300 K. Rectangles highlight the low frequency phase-like mode. For better viewing the spectra have been displaced vertically.

higher temperature, the band becomes less intense and its profile significantly broadens as if a random uncorrelated charge–spin reordering were taking place. A few degrees further below, the band hardens at the onset of a spin pinned charge density wave, perhaps also denoting an incipient spin density wave. The small temperature range for the relatively weak band condensing below T_N prevents us from giving a more quantitative comparison with similar phenomena reported in $R_{1-x}Sr_{1+x}MnO_4$ (R = Nd and La) [33] and for $LaSrMnO_3$ [34]. Nevertheless, and since there is not yet a neutron data counterpart for our compounds, we may extend the discussion in terms of the conclusions drawn by Pailhes *et al* [35] for inelastic neutron scattering measurements in $YMnO_3$. It was found that at low frequencies hybridization takes place due to the mixing of spin waves and phonons. These are well defined zone center features interpreted as multiferroic Goldstone modes. Spin gaps were measured at 2.2 and 5 meV [35]. Very recently, we found that those bands match our lower frequency reflectivity for $RMnO_3$ (R = rare earth) [36]. Accordingly, here we propose that in RMn_2O_5 (R = Pr, Sm, Gd, Tb, Bi), a similar phenomenon is taking place at and below $T_N \sim T_C$. This would involve dislocated, d-orbital e_g electrons being infrared active by dynamical multiferroic coupling. The mode emerging below the ordering transitions, shown in the insets of figure 9, corresponds to this picture.

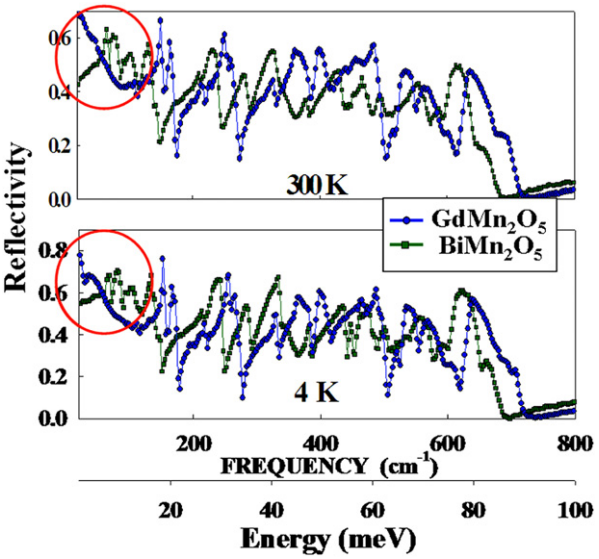

Figure 8. Near normal infrared reflectivity of $GdMn_2O_5$ and $BiMn_2O_5$ at 4 and 300 K. Circles highlight the smooth profile of the low frequency phase-like mode against the discrete phonon spectrum in $BiMn_2O_5$.

As RMn_2O_5 (R = Pr, Sm, Gd, Tb) are insulators, the smooth low frequency band may be simulated above $\sim T_N \sim T_C$ by one dipole. A second one was added to reproduce the partial condensation below transition temperatures.

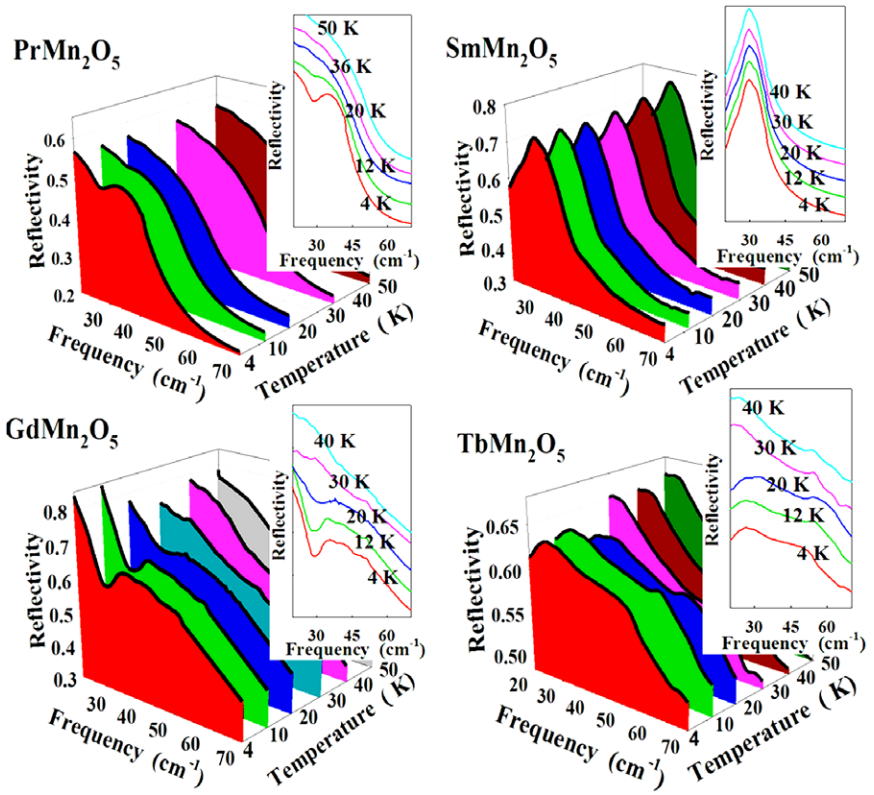

Figure 9. Near normal reflectivity detail of the temperature dependent phase-like mode in RMn_2O_5 (R = Pr, Sm, Gd, Tb). The insets show the same spectra vertically displaced. To ensure reproducibility, some of these measurements were also thermally cycled around $\sim T_N \sim T_C$.

The dielectric function, $\varepsilon(\omega)$ [37], above $\sim T_N \sim T_C$ is then given by

$$\varepsilon(\omega) = \varepsilon_1(\omega) - i\varepsilon_2(\omega) = \varepsilon_\infty \frac{(\omega_{LO}^2 - \omega^2 + i\gamma_{LO}\omega)}{(\omega_{TO}^2 - \omega^2 + i\gamma_{TO}\omega)} \quad (2)$$

where ε_∞ is the high frequency dielectric function; ω_{TO} and $\omega_{LO} = \omega_{\text{'phase-like mode'}}$ are the transverse and longitudinal optical frequencies, and γ_{TO} and $\gamma_{LO}t$ are their dampings, respectively.

The real ($\varepsilon_1(\omega)$) and imaginary ($\varepsilon_2(\omega)$) parts (complex permittivity, $\varepsilon^*(\omega)$) of the dielectric function are then estimated with fits to the data collected in reflectivity measurements using the reflectivity R given by:

$$R(\omega) = \left| \frac{\sqrt{\varepsilon^*}(\omega) - 1}{\sqrt{\varepsilon^*}(\omega) + 1} \right|^2. \quad (3)$$

This procedure allows us to ascertain the real part of the temperature dependent optical conductivity, $\sigma_1(\omega)$, proportional the absorption coefficient [38],

$$\sigma_1(\omega) = \frac{\omega\varepsilon_2}{4\pi}, \quad (4)$$

with maxima at transverse optical frequencies.

The detection of an associated field to longitudinal optical frequencies in near normal reflectivity measurements is a clue to band peaking in the energy loss function:

$$\text{Im}\left(\frac{1}{\varepsilon_1(\omega) + i\varepsilon_2(\omega)}\right). \quad (5)$$

This is verified by angle dependent reflectivity measurements [39].

In addition, we also calculated the strength S_j of the jth oscillator (figure 4) as

$$S_j = \omega_{jTO}^{-2} \frac{(\prod_k \omega_{kLO}^2 - \omega_{jTO}^2)}{(\prod_{k\neq j} \omega_{kTO}^2 - \omega_{jTO}^2)}. \quad (6)$$

Our results for the optical conductivity and the energy loss of $PrMn_2O_5$ at low frequencies are shown in figure 10. They are representative of all our rare earth samples. The temperature dependence of optical conductivity (i.e. transverse excitations) (figure 10(a)) has the same behavior as reported in absorption measurements by Sushkov *et al* [40] and Golovenchits and Sanina (figure 5) [41] in RMn_2O_5 (R = rare earth). It also reproduces the same phonon soft mode hardening when the sample is cooled, as pointed out by Shuvaev *et al* [42] in simpler manganites.

The energy loss spectrum, figure 10(b), peaking at the longitudinal optical frequency undergoes a small softening and narrowing as a consequence of the limited number of electrons experiencing condensation as the material goes through the transition temperatures into the antiferromagnetic–ferroelectric phase.

3.4. Rare earth lattice distortion

The vibrational dependence of rare earths is quantitatively related to a particular property of the internal mode

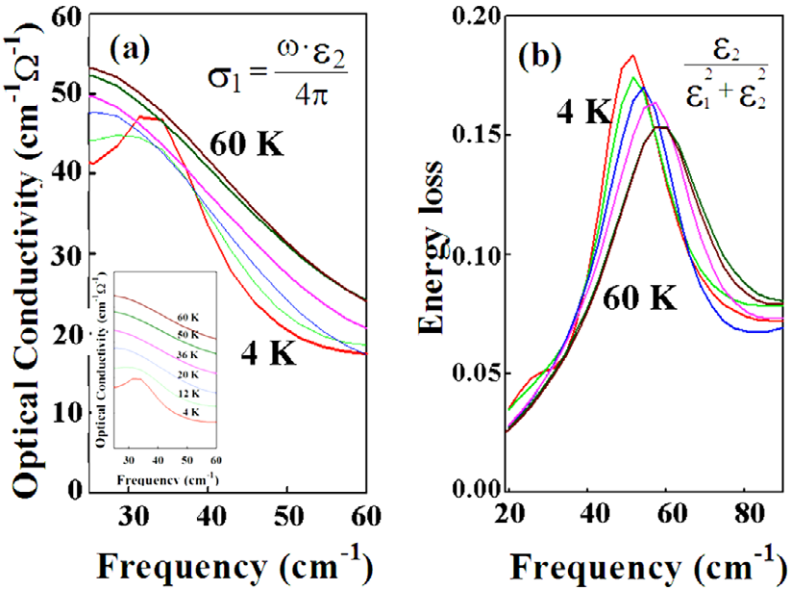

Figure 10. (a) Optical conductivity and (b) energy loss function for the phase-like mode in $PrMn_2O_5$. The inset shows the optical conductivity displaced vertically.

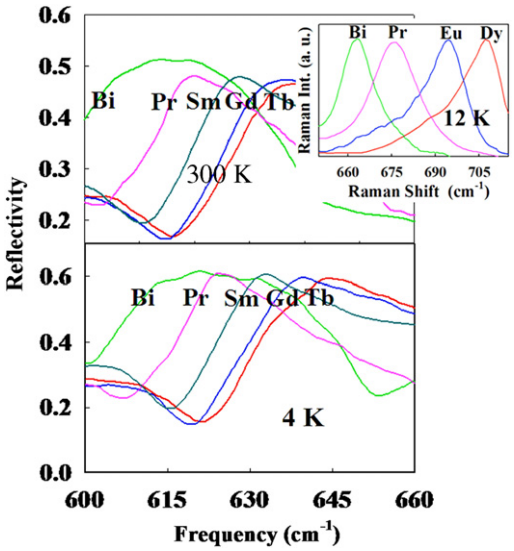

Figure 11. Frequency shifts due to lanthanide contraction in RMn_2O_5 (R = Pr, Sm, Gd, Tb) of the symmetric stretching modes at 300 and 4 K. Inset: Raman spectra of the phonon rare earth dependence at 12 K. For comparison the band corresponding to $BiMn_2O_5$ is also shown in both sets of measurements.

frequencies. As shown in figure 11 for symmetric stretching modes, as the number of electrons in the f shell increases there is an overall hardening of phonon frequencies. This is contrary to what may intuitively be expected from the classical oscillator mass dependence as found for the corresponding bands in the spectra of $BiMn_2O_5$, also shown in figure 11.

We interpret this effect as being due to lanthanide contraction, i.e. as a consequence of the partial screening of f-electrons, 6s-electrons are attracted toward the nucleus decreasing the ionic radius, and consequently stiffening the bonds making the cage and altering the lattice constant systematically [13]. Covalence varies and points to an indirect but first order rare earth dependence of the Mn–O hybridization, because RO_8 cage distortions depend on the rare earth, thus triggering an overall perturbation on nearest neighbor orbitals. Being a structural change, it is easily followed by infrared spectroscopy at all temperatures and is independently verified by Raman scattering (figure 11, inset).

3.5. Discussion

Our far infrared reflectivities (figure 9) suggest activated electric dipoles in the millielectronvolt range of the same nature as those reported by Han *et al* [43] in the paraelectric phase of RMn_2O_5 (R = Tb, Dy, Er) for complex dielectric permittivity using impedance measurements at 100 Hz–1 MHz. They concluded that the thermally activated dipoles were the product of an intrinsic bulk process not involved in magnetically related interactions.

The scenario prompted by our measurements is reminiscent of the collective nature of e_g carriers in colossal magnetoresistance materials and is within the context of charge density waves (CDW) already known in doped manganites. In these systems there is a definitive manifestation of strong electron–lattice coupling creating polaronic carriers, charge hopping, a dynamic Jahn–Teller effect, and an antiferromagnetic background that localizes charges at $T < T_N$ and may lead to regular electronic patterns [1, 44]. In $La_{1-x}Ca_xMnO_3$ ($x = 0.5$, 0.67) the Bardeen–Cooper–Schrieffer (BCS) relation for an optical gap $2\Delta(T)$ opened at $T = T_0$ seems to hold if a ratio $(2\Delta(T_0)/k_BT_C) \sim 5$ is allowed [45].

That implies optical detection of a CDW phase mode and a CDW amplitude mode [46]. The Raman active amplitude mode (CDW position dependent), a soft-phonon-like mode [47, 48] and the far infrared active phase mode

(CDW time dependent), resulting from an electronic cloud beating against the positive background, are paradigmatic excitations of quasi-one-dimensional metals such as blue bronzes $M_{0.3}MoO_3$ (M = K, Rb) [49].

A BCS-type temperature dependence for the gap was also found by Katsufuji *et al* [50] in $La_{1.67}Sr_{0.33}NiO_4$. Here the ratio $2\Delta(0)/K_BT_{CO} \sim 13$ is understood as indicative of unaccounted for electron–electron interactions or fluctuations arising from low dimensionality. This is known for polar manganites, where electrons tend to delocalize in lower dimensional layered structures with strong electron–phonon interactions localizing charge and leading to lattice polarons [51].

However, having verified the absence in RMn_2O_5 (R = rare earth, Bi) of a low frequency Raman excitation in the temperature range 20–300 K, there is need when discussing collective excitations for a broader approach than the BCS single particle excitation across a gap. Keeping a ratio of ∼20 for a gap as in $TbMn_2O_5$ of ∼1.4 eV [52] yields an unrealistically high temperature below which a hypothetical electron quasi-ordered pattern might be triggered.

In RMn_2O_5 (R = rare earth) we are only bound by the detection of a net giant electric dipole created by a fluctuating electronic cloud like a BCS phase mode. The materialization of this electronic cloud interacting as a balance to lattice restoring forces would be the only similarity to the original idea proposed by Fröhlich [53] for a collective mode as consequence of Peierls lattice distortion [54]. On the other hand, as pointed out by Blawid and Millis [55], an extremely large electron–phonon interaction can maintain that picture if localized carriers are considered as polarons, with a large activation gap. This results in a large gap to ordering temperature ratio, and is also consistent with no high temperature metal phase being detected above it.

A source of polaron formation in our compounds is the Mn_2O_{10} Jahn–Teller dimer distortion. The collective band (figure 9) is coincident with Mn^{3+} pyramid 3d superexchange interactions and bond–charge fluctuations in a distorted Mn_2O_{10} complex, where electrons are strongly trapped within Mn sites [56]. This picture also helps to explain the origin of a low energy excitation contribution reported for the near constant thermal expansion coefficient of $BiMn_2O_5$ [25] and the large thermal dependence of Tb–O distances in $TbMn_2O_5$ [30].

The emerging result is thought to be consequence of competition between the tendency of electrons to delocalize in RMn_2O_5 (R = rare earth) and the increase in the charge–lattice interaction, assisted below T_N by the underlying antiferromagnetic order [57, 58]. This is also coincident with the remarkable interrelationship between magnetic and electric polarization properties of the millimeter wave dielectric constant found by Hur *et al* [18]. The magnetically assisted condensation may be the reason why the antiferromagnetic ordering is found always few degrees above the ferroelectric transition. Mn^{3+} e_g electrons, as is already known for simpler octahedral Mn^{3+} manganites [44, 59], will be linked to Jahn–Teller lattice distortions. Polaron fluctuations and condensation at T_N may be interpreted as originating in the Jahn–Teller coupled charge density wave, allowing the detection of an spin density wave below T_N by hybridization. Dislocated d-orbital e_g electrons, that might also be partially spin correlated in the paramagnetic phase, condense in spin wave modes coupled to small atomic displacements, yielding spin–lattice hybrid as measured in $YMnO_3$ [35, 59]. These excitations are detected in the infrared at low frequencies due to complex dynamical multiferroic couplings. Strong Mn–O hybridization is required for spin configuration inducing charge redistribution [52]. This is also supported by oxygen spin polarization measurements at the onset of ferroelectricity, denoting oxygen sites hybridized with Mn^{3+} off-center ions [60].

No substantial changes in crystallographic data are expected when passing $T_N \sim T_C$, and, thus, in the number of phonons detected. The quenched Jahn–Teller orbital in the dimer will locally unveil uncorrelated very weak new internal vibrational modes at low temperatures that will also correlate to the small shifts in the Mn^{3+} lattice position as measured by neutron diffraction [61]. The net weak lattice polarization (ferroelectricity) at $\sim T_C$ would then be a natural consequence.

Summarizing, we report on a far infrared collective phase-like mode and on the origin of the multiferroic phase in RMn_2O_5 (R = Pr, Sm, Gd, Tb, Bi). The deformation of the pyramid sublattice is tied in to the absence of an inversion center in the lower temperature unscreened situation, allowing detection of weak spontaneous lattice polarization (ferroelectricity). This is due to electron condensation taking place in the system assisted by the magnetic ordering in an already higher temperature non-centrosymmetric space group. At T_N and below, there are no substantial changes in crystallographic data described by an x-ray effective *Pbam* space group, and accordingly no change in the number of phonons measured across $\sim T_N \sim T_C$. As RMn_2O_5 (R = rare earth, Bi) is structurally close to a layered topology, strong localized and correlated polarons, as suggested by the ∼0.4 eV tail in the $TbMn_2O_5$ reported optical gap of ∼1.4 eV [52], could play a significant role. Conclusions from recent calculations on the structure and ferroelectric polarization of $TbMn_2O_5$ support the view of a charge/orbital ordered ground state driven by the octahedra and pyramids where the main role in the polarization is due to Mn^{3+} ions in the pyramids. It also points to the magnetic structure assisting the lattice polarization (ferroelectricity) in agreement with our proposition [62].

Lanthanide contraction causes phonon hardening as the number of f-electrons increases and may introduce a systematic orbital perturbation.

Acknowledgments

NEM is grateful to the CNRS-CEMHTI laboratory and staff in Orléans, France, for research and financial support in performing far infrared measurements. NEM, GFLF, GMA would like to thank the Brazilian Synchrotron Light Laboratory (Laboratorio Nacional de Luz Sincrotron, LNLS) for economic assistance and making available

beam time at the D04B-XAFS1 beamline. LDC thanks the Basque Government for post-doctoral financial support at the CNRS-CEMHTI NEM also acknowledges partial financial support (PIP 0010) from the Argentinean Research Council (Consejo Nacional de Investigaciones Científicas y Técnicas-CONICET). Funding through Spain Ministry of Science and Innovation (Ministerio de Ciencia e Innovación) under project no. MAT2010-16404 is acknowledged by JAA and MJM-L.

References

[1] Resnik D 2012 arXiv:1202.0852
[2] Goldstone J, Salam A and Weinberg S 1962 *Phys. Rev.* **127** 965
[3] de Souza R and Moore J E 2008 *Phys. Rev.* B **77** 012406
[4] Katsura H, Balarsky A V and Nagaosa N 2007 *Phys. Rev. Lett.* **98** 027300
[5] Mostovoy J 2006 *Phys. Rev. Lett.* **96** 067601
[6] Pimenov A, Shuvaev A M, Mukhin A A and Loidt A 2008 *J. Phys.: Condens. Matter* **20** 434209
[7] Lines M E and Glass A M 1977 *Principles and Applications of Ferroelectrics and Related Materials* (Oxford: Clarendon)
[8] Stern E A 2004 *Phys. Rev. Lett.* **93** 037601
[9] Wang K F, Liu J M and Ren Z F 2008 *Adv. Phys.* **58** 321
[10] Massa N E, del Campo L, De Sousa Meneses D, Echegut P, Frabbris G F L, Azevedo G, Martínez-Lope M-J and Alonso J A 2010 *J. Appl. Phys.* **108** 084114
[11] Ribeiro J L 2007 *Phys. Rev.* B **76** 144417
[12] Alonso J A, Casais M T, Martinez-Lope M-J and Rasines J 1997 *Solid State Chem.* **129** 105
[13] Muñoz A, Alonso J A, Casais M-T, Martínez-Lope M J, Martínez J L and Fernández-Diaz M T 2005 *Eur. J. Inorg. Chem.* **2005** 685
[14] Alonso J A, Casais M T, Martínez-Lope M J, Martínez J L and Fernández-Díaz M T 1997 *J. Phys.: Condens. Matter* **9** 8515
[15] Chapon L G, Radaelli P G, Blake G R, Park S and Cheong S-W 2006 *Phys. Rev. Lett.* **96** 097601
[16] Muñoz A, Alonso J A, Casais M T, Martinez-Lope M J, Martinez J L and Fernández-Diaz M T 2002 *Phys. Rev.* B **65** 144423
[17] Kobayashi S, Osawa T, Kimura H, Noda Y, Kagomiya I and Kohn K 2004 *J. Phys. Soc. Japan* **73** 1593
[18] Hur N, Park S, Sharma P A, Guha S and Cheong S-W 2004 *Phys. Rev. Lett.* **93** 107207
[19] Kagomiya I, Matsumoto S, Kohn K, Fukuda Y, Shoubu T, Kimura H, Noda Y and Ikeda N 2006 *Ferroelectrics* **286** 167
[20] Volkova L M and Marinin D V 2009 *J. Phys.: Condens. Matter* **21** 5903
[21] Mihalova B, Gospodinov M M, Guthler B, Yen F, Liyvinchuk A P and Live M N 2005 *Phys. Rev.* B **71** 172301
[22] García-Flores A F, Granado E, Martinho H, Urbano R R, Rettori C, Golovenchits E I, Sanina V A, Oseroff S R, Park S and Cheong S-W 2004 *Phys. Rev.* B **73** 104411
[23] Efremov D V, Van den Brink J and Khomskii D I 2004 *Nature Mater.* **3** 853
[24] García-Flores A F, Granado E, Martinho H, Urbano R R, Rettori C, Golovenchits E I, Sanina V A, Oseroff S R, Park S and Cheong S-W 2007 *J. Appl. Phys.* **101** 09M106
[25] Granado E, Eleotério M S, García-Flores A F, Sopuiza J A, Golovenchits E I and Sanina V A 2008 *Phys. Rev.* B **77** 134101
[26] Litvinchuk A J 2009 *J. Magn. Magn. Mater.* **312** 2373
[27] Cao J, Vergara L I, Musfeldt J L, Litvinchuk A J, Wang Y-J, Park S and Cheong S-W 2008 *Phys. Rev.* B **78** 064307
[28] Koningsberger D C and Prins R (ed) 1988 *X-Ray Absorption: Principles, Applications, Techniques of EXAFS, SEXAFS and XANES* (New York: Willey)
[29] Fabbris G F L 2009 *MSc Thesis* Institute of Physics, Universidade Estadual de Campinas, Campinas, Brazil
[30] Tyson T, Deleon M, Yoong S and Cheong S-W 2007 *Phys. Rev.* B **75** 174413
[31] Valdés Aguilar R, Sushkov A B, Park S, Cheong S-W and Drew H D 2006 *Phys. Rev.* B **74** 184404
[32] Seshadri R and Hill N A 2001 *Chem. Mater.* **13** 2892
[33] Fujioka J, Ida Y, Takahashi Y, Kida N, Shimano R and Tukura Y 2010 *Phys. Rev.* B **82** 140409R
[34] Nucara A, Maselli P, Calvani P, Sopracase R, Ortolani M, Gruener G, Cestelli Guidi M, Schade U and Garcia J 2008 *Phys. Rev. Lett.* **101** 066407
[35] Pailhès S, Fabrèges X, Régnault L P, Pinsard-Godart L, Mircheau I, Moussa F, Hennion M and Petit S 2009 *Phys. Rev.* B **79** 134409
[36] Massa N E, del Campo L, De Sousa Meneses D, Echegut P, Martínez-Lope M J and Alonso J A 2012 *Bull. Am. Phys. Soc.* **17** 1
[37] Kurosawa T 1961 *J. Phys. Soc. Japan* **16** 1298
[38] Wooten F 1972 *Optical Properties of Solids* (San Diego, CA: Academic)
[39] Berreman D W 1963 *Phys. Rev.* **130** 2193
See also, Massa N E, Denardin J C, Socolovsky M, Knobel M and Zhang X X 2009 *J. Appl. Phys.* **105** 114306
[40] Sushkov A B, Valdés Aguilar R, Park S, Cheong S-W and Drew H D 2007 *Phys. Rev. Lett.* **98** 027202
[41] Golovenchits E and Sanina Y 2004 *J. Phys.: Condens. Matter* **16** 4325
[42] Shuvaev A M, Hemberg J, Niemann D, Schrette F, Loidl A, Yu V, Ivanov J, Travkin V, Mukhin A A and Pimenov A 2010 *Phys. Rev.* B **52** 174417
[43] Han T C, Lin J G, Kuo K M and Chem G 2008 *J. Appl. Phys.* **103** 084106
[44] Tokura Y 2006 *Rep. Prog. Phys.* **69** 797
[45] Calvani P, de Marzi G, Dore P, Lupi S, Maselli P, d'Amore F and Gagliardi S 1998 *Phys. Rev. Lett.* **81** 4504
[46] Gruner G 1988 *Rev. Mod. Phys.* **60** 1129
[47] Travaglini G, Mörke I and Wachter P 1983 *Solid State Commun.* **45** 289
[48] Massa N E 1990 *Solid State Commun.* **76** 805
[49] Travaglini G and Wachter P 1984 *Phys. Rev.* B **30** 1971
[50] Katsufuji T, Tanabe T, Ishikawa T, Fkuda Y, Arima T and Tokura Y 1996 *Phys. Rev.* B **54** 14230
[51] Zaanen J and Littlewood P B 1994 *Phys. Rev.* B **50** 7222
[52] Moskin S and Pisarev R V 2008 *Phys. Rev.* B **77** 060102(R)
[53] Fröhlich H 1954 *Proc. R. Soc.* A **223** 269
[54] Peierls R E 1955 *Quantum Theory of Solids* (Oxford: Clarendon)
[55] Blawid S and Millis A 2000 *Phys. Rev.* B **62** 2424
[56] Daoud-Aladine A, Rodrigues-Carvajal J, Pinsard-Gaudart L, Fernández-Díaz M T and Revcolevschi A 2002 *Phys. Rev. Lett.* **89** 097205
[57] Golovenchits E I, Morozov E V, Sanina V-A and Sapozhnikova L M 1992 *Sov. Phys.—Solid State* **34** 56
[58] Campbell B J, Osborn R, Argyriou D N, Vasilu-Doloc I, Mitchell J F, Sinha S K, Ruett U, Ling C D, Island Z and Lynn J W 2001 *Phys. Rev.* B **65** 014427
[59] Sato J, Lee S H, Katsufuji T, Mesaki M, Park S, Copely J R D and Takagi H 2003 *Phys. Rev.* B **68** 014432
[60] Beale T-A-W, Wilkins S B, Johnson R D, Bland S R, Joly Y, Forrest T R, McMorrow D F, Yakhou F, Prabhakaran D, Boothroyd A T and Hatton P D 2010 *Phys. Rev. Lett.* **105** 087203
[61] Blake G R, Chapon L C, Radaelli P G, Park S, Hur N, Cheong V and Rodriguez-Carvajal J 2003 *Phys. Rev.* B **71** 214402
[62] Chang T-R, Jeng H-T, Ren C-Y and Hsue C-S 2011 *Phys. Rev.* B **84** 024421